New Journal of Physics
The open access journal at the forefront of physics

Deutsche Physikalische Gesellschaft DPG
IOP Institute of Physics

Published in partnership with: Deutsche Physikalische Gesellschaft and the Institute of Physics

OPEN ACCESS

RECEIVED
2 July 2018

REVISED
16 November 2018

ACCEPTED FOR PUBLICATION
10 December 2018

PUBLISHED
28 February 2019

PAPER

Limitations of rotating-wave approximation in magnetic resonance: characterization and elimination of the Bloch–Siegert shift in magneto-optics

J I Sudyka[1], S Pustelny and W Gawlik

Marian Smoluchowski Institute of Physics, Jagiellonian University, Łojasiewicza 11, 30-348, Kraków, Poland
[1] Current address: Institute of Physical Chemistry, Polish Academy of Sciences, Kasprzaka 44/52 01-224 Warszawa, Poland.

E-mail: pustelny@uj.edu.pl

Keywords: Bloch–Siegert effect, rotating-wave approximation, magneto-optical effect, magnetometry, alkali-metal vapors

Abstract

We present investigations of radio-frequency (RF) resonances observed in an optically pumped rubidium vapor. By measuring the systematic shifts (the Bloch–Siegert shifts) of RF resonances in low magnetic fields, we demonstrate limitations of the rotating-wave approximation in the case of angular momentum $F \geqslant 1$. The resonance shifts and deformations are characterized in a wide range of parameters and it is shown that the observed behavior is far more complex than in a standard two-level system. It is also demonstrated that the shifts can be controllably turned on or off by switching between the oscillating and rotating magnetic field. Experimental results are supported with numerical calculations, reproducing all features of the observed signals. Besides fundamental aspect of the research, application of rotating magnetic field helps to suppress/evaluate spectroscopic-measurement and precise-metrology systematic errors. The reported study has also important implications for quantum metrology and information processing beyond RWA and standard two-state qubit dynamics.

1. Introduction

A standard treatment of a two-level system interacting with a resonant electromagnetic field is based on decomposition of an oscillating field into two counter-rotating components and consideration of system's interaction with only one of them. This approach, known as rotating-wave approximation (RWA), is justified in most cases, such as not-too-strong or optical fields, i. e. when the field-atom coupling strength is a small fraction of bare frequency of an uncoupled atom. In a particular case of oscillating magnetic field $\boldsymbol{B}_{\mathrm{RF}}\cos(\omega t)$ applied to polarized atoms immersed in perpendicularly oriented static magnetic field $\boldsymbol{B_0}$, the interaction leads to appearance of the resonance at frequency Ω_r. In RWA, Ω_r equals the static-field Larmor frequency $\Omega_0 = g\mu_{\mathrm{B}}B_0/\hbar$, where g, μ_B, $\hbar$ are the gyromagnetic ratio, the Bohr magneton, and the reduced Planck constant, respectively. However, due to interaction with a counter-rotating component of the oscillating magnetic field, the actual resonance position is shifted from Ω_0. The lowest-order approximation of this shift was primarily derived by Bloch and Siegert [1] and is given by

$$\Delta\Omega = \Omega_0 - \Omega_r \approx \frac{\Omega_{\mathrm{RF}}^2}{16\Omega_0}, \tag{1}$$

where $\Omega_{\mathrm{RF}} = g\mu_B B_{\mathrm{RF}}/\hbar$. $\Delta\Omega$ is known as the Bloch–Siegert shift (BSS).

Since its first description in 1940 [1], BSS was carefully investigated theoretically [2–4] to develop analytical solution for $\Delta\Omega$. Experimental studies of the effect were performed with different electron-spin [5, 6], as well as, nuclear-spin systems [7, 8]. Recently, the effect was revisited for novel applications in quantum metrology [9] and quantum information processing [10–12]. In the latter case, the interest is motivated by the need to perform coherent control of a quantum system with possibly short electromagnetic pulses to reach high bandwidth of

system's manipulation. Since it is the pulse area that determines coherent evolution of the Bloch vector, shortening of the pulses must be done by corresponding increase of their amplitudes, which makes BSS more important. Consequently, for strong driving fields, when the shift becomes comparable with the eigenfrequency of the system (the Larmor frequency in our case), significant departures from RWA hinder coherent control of the qubits because of complex, nonharmonic Rabi oscillations. Recent work with superconducting circuits [10, 11] and nitrogen-vacancy centers in diamonds [13, 14] demonstrate that this difficulty can be successfully alleviated. The BSS appears important also for experiments with cold atoms in dressed and adiabatic potentials [15–17]. An interplay between the Bloch–Siegert and AC Stark effects has been studied and applied to control valleytronic properties of novel 2D materials like monolayer WS_2 (see [18] and references therein).

Despite growing importance of BBS, to our knowledge, the effect has not been taken into consideration in studies of nonlinear magneto-optical effects in alkali metal vapors [19, 20] (although some estimates were given in [21]). Since these phenomena are widely used in modern quantum metrology, we find that thorough analysis of BSS is crucial to avoid systematic errors in precision magnetometry and spectroscopic measurements with warm and cold atoms [22, 23].

In this paper, we present both experimental and theoretical (numerical) studies of BSS in a Rb vapor system subjected to static and oscillating/rotating magnetic fields. The effect is studied by means of radio-frequency (RF) nonlinear magneto-optical rotation (NMOR) [24, 25], where resonances are created and detected via properly tuned linearly-polarized laser light interplaying with static and oscillating magnetic fields. NMOR is based on optical detection of medium's anisotropy (birefringence and/or dichroism) caused by magnetic perturbations of optically polarized medium. The perturbation may change populations and coherences of the atomic system, so the method is useful for sensitive monitoring of atomic states and their superpositions [23, 26]. Important features of our system are: a possibility of application of either rotating or oscillating magnetic field under otherwise the same experimental conditions, generation of narrow ($\approx$1 Hz) RF NMOR resonances, and measurements at ultra-low alternating- (RF-) field frequencies ($\omega/2\pi = 1$–100 Hz). The first aspect is essential for elimination of systematic errors, while the second and third are relevant because of inverse proportionality of the shift to the magnitude of static (DC) magnetic field (equation (1)). Precision of our method, enhanced by the small value of Ω_0, enables utilization of much weaker RF fields than in previous experiments. Hence, in our case the perturbative approach derived in [2–4] is valid. Exerting strong RF fields to reach the limit where perturbation method is no longer credible (i.e. $\Omega_{\mathrm{RF}} \gtrsim 2.4\Omega_0$) leads to broadening and deformation of resonance lineshapes, and thus reduced precision of the measurement [2, 4].

In RF NMOR, RWA is typically applied with respect to all oscillating fields (optical and magnetic) and BSS is disregarded. Herein, the second approximation is not used. Moreover, in contrast to most previous studies with spin 1/2, we analyze the case of angular momentum $F \geqslant 1$. In that case, a strong RF field ($\Omega_{\mathrm{RF}} \gtrsim \Omega_0$) reveals important interference effect. The effect goes beyond the standard two-state qubit dynamics and enters the avenues to generate and control more sophisticated superposition states, like qutrits, qunits, etc [27].

2. Numerical approach

We investigate BSS of NMOR resonances using the density-matrix formalism and a model atomic system with the $F = 1$ ground state and the $F' = 0$ excited state, interacting with linearly polarized light and immersed in AC and DC magnetic fields (figure 1). Despite its simplicity, this is a generic system for most NMOR experiments. The Hamiltonian of the system is presented in a rotating frame, corresponding to the optical frequency ω_{light}, which is the only approximation used in our numerical modeling. In the $|F,\ m_F\rangle$ base, with a quantization axis along the light propagation direction (z) but perpendicular to the static magnetic field, the Hamiltonian of the system under consideration is given by

$$H = H_0 + H_E + H_B, \tag{2}$$

$$H_0 = \hbar\Delta\begin{bmatrix}0&0&0&0\\0&0&0&0\\0&0&0&0\\0&0&0&1\end{bmatrix}, \quad H_E = -\boldsymbol{d}\cdot\boldsymbol{E}_{\mathrm{lin}} = \frac{\mathrm{i}\hbar\beta}{2}\begin{bmatrix}0&0&0&-1\\0&0&0&0\\0&0&0&-1\\1&0&1&0\end{bmatrix}, \tag{3}$$

where $\boldsymbol{d}$ is the electric dipole moment of the optical transition, $\boldsymbol{E}_{\mathrm{lin}}$ is the light vector of an amplitude, $\Delta = \omega_0 - \omega_{\mathrm{light}}$ is the laser frequency detuning, and $\beta = -\mathrm{d}E_{\mathrm{lin}}/\hbar$ is the optical Rabi frequency. For the the magnetic field composed of the static and oscillating magnetic field, $\boldsymbol{B}_{\mathrm{lin}} = \hbar/(g\mu_B)[0,\ \Omega_0,\ \Omega_{\mathrm{RF}}\cos(\omega t)]^T$, the magnetic Hamiltonian $H_B = -\boldsymbol{\mu}\cdot\boldsymbol{B}$, where $\boldsymbol{\mu}$ is the magnetic dipole moment, takes the form

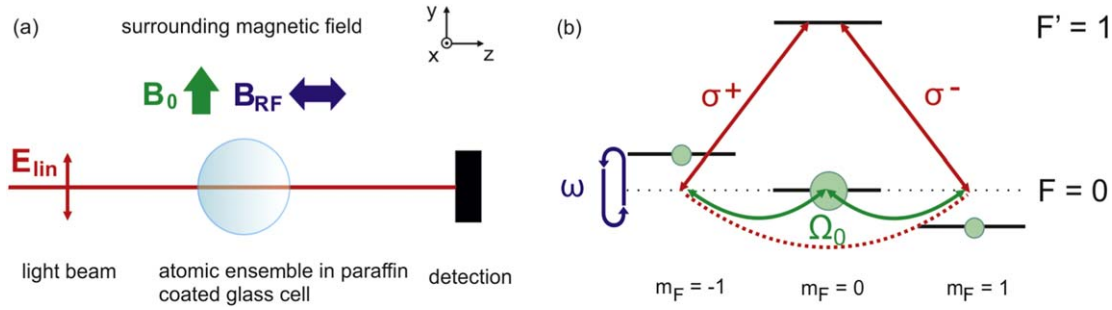

Figure 1. (a) Geometry of the experiment. The y-polarized light $E_{\rm lin}$ passes the glass cell filled with rubidium vapor along z. The atoms are immersed in the static, y-oriented magnetic field $\boldsymbol{B_0}$ and the oscillating, z-oriented magnetic field $\boldsymbol{B}_{\rm RF}$. Polarization of light is measured after the medium with a polarimeter. (b) Energy-level structure, along with the couplings, in the model system (quantization axis along z). Ground-state population distribution is marked with dots. The ground-state coherences $\Delta m = 1$ are generated with the DC magnetic field (solid green arrows) and the coherences $\Delta m = 2$ by the optical field decomposed into $\sigma^{\pm}$(red dotted arrow). The AC magnetic field induces periodic changes in the Zeeman splittings of the magnetic sublevels, modulating light detuning and hence birefringence of the medium with frequency ω, as marked by looping arrows.

$$H_B^{\rm lin} = \hbar \begin{bmatrix} \Omega_{\rm RF}\cos(\omega t) & \frac{-i\Omega_0}{\sqrt{2}} & 0 & 0 \\ \frac{i\Omega_0}{\sqrt{2}} & 0 & \frac{-i\Omega_0}{\sqrt{2}} & 0 \\ 0 & \frac{i\Omega_0}{\sqrt{2}} & -\Omega_{\rm RF}\cos(\omega t) & 0 \\ 0 & 0 & 0 & 0 \end{bmatrix}. \tag{4}$$

In the case of the rotating magnetic field $\boldsymbol{B}_{\rm rot} = \hbar/(g\mu_B)\left[\frac{\Omega_{\rm RF}}{2}\sin(\omega t),\ \Omega_0,\ \frac{\Omega_{\rm RF}}{2}\cos(\omega t)\right]^T$, H_B is given by

$$H_B^{\rm rot} = \hbar \begin{bmatrix} \frac{\Omega_{\rm RF}}{2}\cos(\omega t) & \frac{-i\Omega_0}{\sqrt{2}} + \frac{\Omega_{\rm RF}}{2\sqrt{2}}\sin(\omega t) & 0 & 0 \\ \frac{i\Omega_0}{\sqrt{2}} + \frac{\Omega_{\rm RF}}{2\sqrt{2}}\sin(\omega t) & 0 & \frac{-i\Omega_0}{\sqrt{2}} + \frac{\Omega_{\rm RF}}{2\sqrt{2}}\sin(\omega t) & 0 \\ 0 & \frac{i\Omega_0}{\sqrt{2}} + \frac{\Omega_{\rm RF}}{2\sqrt{2}}\sin(\omega t) & -\frac{\Omega_{\rm RF}}{2}\cos(\omega t) & 0 \\ 0 & 0 & 0 & 0 \end{bmatrix}. \tag{5}$$

The density-matrix evolution is described by the Liouville equation

$$i\hbar\frac{d\rho}{dt} = [H,\ \rho] - i\hbar\{\Gamma,\ \rho\} + i\hbar\Lambda, \tag{6}$$

where Γ and Λ are the relaxation and repopulation operators given by:

$$\Gamma = \begin{bmatrix} \gamma & 0 & 0 & 0 \\ 0 & \gamma & 0 & 0 \\ 0 & 0 & \gamma & 0 \\ 0 & 0 & 0 & \gamma+\gamma_e \end{bmatrix},\quad \Lambda = \frac{\gamma+\gamma_e\rho_{00}}{3}\begin{bmatrix} 1 & 0 & 0 & 0 \\ 0 & 1 & 0 & 0 \\ 0 & 0 & 1 & 0 \\ 0 & 0 & 0 & 0 \end{bmatrix}. \tag{7}$$

ρ_{00} is the excited-state population and $\gamma/(2\pi) = 1$ Hz and $\gamma_e/(2\pi) = 6$ MHz are typical values of respective ground- and excited-state relaxation rates of ^{85}Rb atoms in a paraffin-coated vapor cell. In the model, no atomic kinematics, like thermal motion of atoms, is taken into account.

By solving equation (6) numerically[2], time evolution of the density matrix and all necessary observables can be calculated based on the medium's polarization [28]

$$\boldsymbol{P} = N\,\mathrm{Tr}(\rho\boldsymbol{d}), \tag{8}$$

where N is the number density of atoms. From the polarization P one can calculated the observable relevant for NMOR, i.e. the angle of polarization rotation ϕ, can be related to the medium's optical anisotropy. The angle is determined by the difference between refractive indices of two circular components of linearly polarized light. As the indices are related to the optical coherence between specific sublevels, in our system, the polarization rotation angle ϕ is given by

$$\phi \propto \mathrm{Im}(\rho_{-10} - \rho_{10}), \tag{9}$$

where ρ_{-10} (ρ_{10}) is the optical coherence between the $|1,\ -1\rangle$ ($|1,\ 1\rangle$) ground state and the $|0,\ 0\rangle$ excited state. Time dependence of $\boldsymbol{B}_{\rm RF}(t)$ results in modulation of the rotation angle ϕ. To reproduce measurements of the

[2] Numerical calculations were performed by means of *Atomic Density Matrix* package [29] in *Wolfram Mathematica* computing environment.

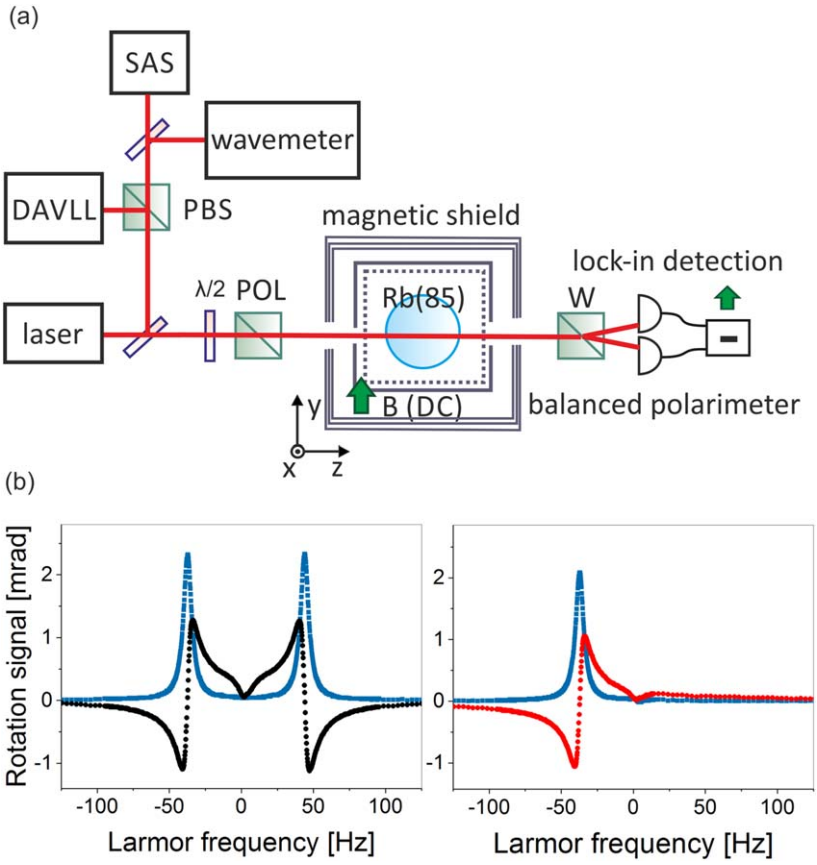

Figure 2. (a) Experimental setup and (b) RF NMOR signals observed at low Ω_{RF}. ^{85}Rb ensemble is optically pumped and probed by linearly polarized light tuned to the low-frequency wing of the Doppler-broadened $F = 3 \rightarrow F'$ transition. A set of coils produces the leading magnetic field $\boldsymbol{B_0}$ in the y direction and the time-dependent magnetic field $\boldsymbol{B}_{RF}$ in the x and/or z direction. The polarization rotation is measured with a balanced polarimeter and a lock-in amplifier. DAVLL stands for the dichroic atomic vapor laser lock, SAS is the saturated absorption spectroscopy, PBS is the polarizing beam splitter, W is the Wollaston prism, $\lambda/2$ denotes the half-wave plate used with a Glan–Thompson polarizer (POL) for the light power adjustment. The rotation signals are recorded with a computer (not shown). (b) The in-phase (black/red or grey) and quadrature (blue or dark grey) components of the recorded resonances for oscillating (left) and rotating (right) magnetic fields. The AC field frequency is held constant while the static magnetic field is scanned.

light parameters with the phase-sensitive detection, time-dependent solutions of the polarization rotation is are integrated over the period $T = 2\pi/\omega$ at the time t_S needed for the system to approach the steady state

$$\phi_{\mathrm{p}}(\omega) + \mathrm{i}\phi_{\mathrm{q}}(\omega) = \int_{t_S}^{t_S+T} \phi(\tau)\exp(\mathrm{i}\omega\tau)\,\mathrm{d}\tau, \tag{10}$$

where subscripts p and q correspond to the signal measured in phase and in quadrature with the AC magnetic field.

3. Experimental setup

The central part of our experimental setup (figure 2(a)) is a spherical, paraffin-coated vapor cell of 10 cm diameter filled with isotopically enriched ^{85} Rb (longitudinal relaxation time ≈ 1 s) at room temperature. The cell is surrounded by a three-layer magnetic shielding made of μ-metal and a ferrite cube as an additional innermost layer. The shielding is able to reduce residual magnetic fields by four orders of magnitude (from Earth's magnetic field of $\sim$1 G (10^{-4} T) to $\sim$100 μG (10^{-8} T)) in a wide range of frequencies [30]. A set of magnetic-field coils generating homogeneous magnetic fields in all three directions is mounted inside the shield. The leading field is set along the y axis. Other coils serve for passive compensation of residual fields and are used to generate a variable magnetic field[3]. In case of oscillating field, one of the perpendicular coils (x or z) is fed with a sinusoidal signal. The rotating field is produced when $\cos(\omega t)$ and $\sin(\omega t)$ signals are applied to x and z coils,

[3] The cell construction and field homogeneity enable observation of narrow ($\lesssim$1 Hz) resonances, which is essential for precise measurements. On the other hand, the efficient magnetic shielding and compensation make it possible to measure resonances at ultra-low frequencies ($\lesssim$100 Hz), corresponding to DC magnetic fields of about 100 μG (10^{-8} T) or smaller.

respectively. Due to imperfect symmetry between the coils some degree of ellipticity may be present in the rotating field. We mitigate this effect by optimizing rf field amplitude and phase in x coil (see below).

Linearly polarized laser beam tuned to the $D1$ (795 nm) line of rubidium creates spin alignment and monitors atomic polarization changes induced by magnetic fields. It is tuned to a wing of the Doppler broadened $F = 3 \rightarrow F'$ transition (detuned -260 MHz from the $F = 3 \rightarrow F' = 2$ transition). The laser light frequency is stabilized with a dichroic atomic vapor laser lock [31, 32] and a saturated absorption spectroscopy system serves as frequency reference. Typical light power[4] prior the cell is 20 μW (in paraffin-coated cells, the power is averaged over the cell volume [33]). Polarization rotation is detected by a balanced polarimeter. The signal is demodulated with a lock-in amplifier, operating at the RF field frequency typically between 1 and 100 Hz.

The RF NMOR signals obtained by sweeping the static magnetic field with a fixed RF-field frequency and amplitude are presented in figure 2(b). The Larmor frequency Ω_0 corresponding to the static field is extrapolated from an independent calibration based on relation between the current applied to the calibrated coil and the resonance frequency in a high-frequency regime with low AC-field amplitude. The oscillating field generates two resonances at $\pm\Omega_r$, where the sign denotes the conventional precession and static magnetic field direction/handedness of RF field, whereas a single resonance at Ω_r occurs with the rotating field. In case of the latter, to ensure good quality of rotating field we adjusted the amplitude and phase of magnetic field in x coil to see minimum amplitude residual signal at $-\Omega_r$. In that manner we achieved $<2\%$ degree of ellipticity, measured as ratio between two signals' amplitude. The in-phase component of the observed resonances is characterized by the dispersive shape, while its quadrature counterpart is absorptive. Width of both resonances is determined by the ground-state relaxation rate. A small dip around $\Omega_0 = 0$ is considered as an experimental singularity caused by $1/f$ noise in the system[5].

The drawback of the scheme with a fixed RF-field frequency is the necessity of scanning the static magnetic-field amplitude; due to the change in operation conditions of the current source, magnetic-field scanning may introduce uncertainties to the measurements (magnetic-field drifts). To avoid this problem, further results are taken with a constant static magnetic field (more stable operation conditions) and the RF-field frequency ω is swept discretely (point by point with 1 s intervals between successive measurements, related to lock-in integration time of 300 ms) around the resonance frequency ω_r. The RF-field amplitude remains constant for each scan. A restriction of such a scheme is the ability of scanning only the positive frequencies of the RF field.

4. Results

Figure 3 presents numerical (derived from equations (9) and (10)) and experimental signals (in-phase component) generated with the oscillating and rotating fields at three distinct AC-field amplitudes (expressed in terms of the Rabi frequency Ω_{RF})[6]. At low Ω_{RF}, the shape of the NMOR resonance is purely Lorentzian. When the AC field becomes stronger the resonance broadens and a new narrow structure develops in its center. This effect does not occur for standard two-level structures, where the signal broadens but remains a single Lorentzian. The so-called Majorana reversal is characteristic for systems with $F \geqslant 1$. It was observed and first described in [34], however its rigorous calculation was derived primarily by Majorana [35]. Consistent analytical results were obtained in [36], where the most general case of AC and DC magnetic fields orientation was studied and approximation methods were used. The effect was interpreted as the result of quantum interference between one- and three-photon processes, each contributing to the resonance with a different linewidth and amplitude depending on Ω_{RF} [37]. The resonance lineshapes, including the Majorana reversal for RF NMOR, were calculated in [38] and we use them in our fitting procedure in the following form

$$\phi_{\mathrm{p}}(\omega) = \frac{\phi_0\omega\Omega_{\mathrm{RF}}[\gamma^2 - 2\Omega_{\mathrm{RF}}^2 + 4(\omega-\omega_r)^2]}{[\gamma^2 + \Omega_{\mathrm{RF}}^2 + (\omega-\omega_r)^2][\gamma^2 + 4\Omega_{\mathrm{rf}}^2 + 4(\omega-\omega_r)^2]},$$
$$\phi_{\mathrm{q}}(\omega) = \frac{\phi_0\Omega_{\mathrm{RF}}[\gamma^2 + \Omega_{\mathrm{RF}}^2 + 4(\omega-\omega_r)^2]}{[\gamma^2 + \Omega_{\mathrm{RF}}^2 + (\omega-\omega_r)^2][\gamma^2 + 4\Omega_{\mathrm{RF}}^2 + 4(\omega-\omega_r)^2]}, \quad (11)$$

where ϕ_0 is the amplitude of the magneto-optical rotation.

[4] The light power should be sufficiently low to reduce possible power broadening of observed resonances.

[5] Modeling without the noise does yield signals without the central zero-field feature, but adding pink noise reproduces faithfully the signals of the figure 1(a). It was also experimentally verified that the width of the central dip increases with the vapor temperature (which confirms thermal origin of the noise).

[6] Ω_{RF} was calibrated with a separate measurement. $V(t) = V_{\mathrm{RF}} + V_{\mathrm{RF}}\cos(\omega t)$ signal was applied to the z coil and the resonance frequency $\Omega_{\mathrm{RF}}/(2\pi)$ was measured.

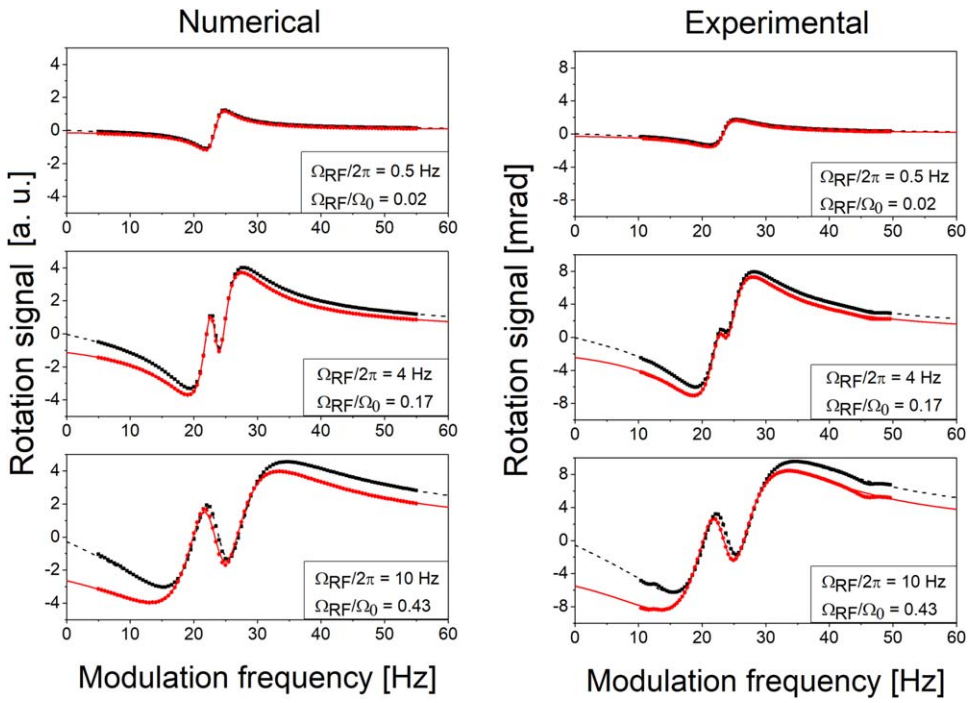

Figure 3. Numerical (left) and measured (right) NMOR signals for oscillating (black squares) and rotating magnetic fields (red or grey dots) along with fitted Majorana reversal NMOR functions (dashed and solid lines, respectively) (equations (11)) for three different AC magnetic field strengths indicated in right bottom corner of each graph. The static magnetic field $\boldsymbol{B_0}$ was set in such a way that $\Omega_0/(2\pi) = 23$ Hz. Residual magnetic fields are responsible for appearance of weak resonances at $\omega_r/2$ and $2\omega_r$ observed in the experimental data for high Ω_{RF}. Statistical error bars are smaller than the graph marker.

The correct description of RF NMOR with oscillating magnetic field requires taking into account the counter-rotating component of linearly polarized light, which is associated with the second resonance at the negative frequency $-\Omega_r$ (not observed directly in the experiment). Omission of the resonance would lead to systematic algebraic shifts. Figure 3 shows that for stronger AC fields, small features at $\omega_r/2$ and $2\omega_r$ are observed in experimental signals. We attribute the features to the residual, not fully compensated, transverse magnetic fields[7], which may tilt the resulting $\boldsymbol{B_0}$ direction. As a consequence, the quantization axis may no longer be perpendicular to the static magnetic field and this would produce additional small harmonic and subharmonic resonances. This interpretation is consistent with our numerical simulations of resonances in tilted fields. We fit those residual signals with small absorptive resonances with predefined positions ($\omega_r/2$ and $2\omega_r$) and a given width. The residual fields cause also a small mixing between two lock-in channels (in-phase and quadrature), which is taken into account by fitting the experimental data with a combination of the resonance shapes given by equations (11). In case of the rotating-field-induced resonance, residual fields are exclusively responsible for the mixing. When such a resonance is considered, an additional phase mixing is produced by counter-rotating component of the AC field (interference of the measured resonance with the tail of the resonance at $-\Omega_r$).

For quantitative measurements of the Bloch–Siegert effect, we focused on the difference between resonance frequencies when the driving field is either oscillating or rotating, $\Delta\omega = \omega_r^{\mathrm{rot}} - \omega_r^{\mathrm{lin}}$, and regarded this difference as the measure of BSS. In figure 3, the measured and simulated values of $\Delta\,\omega$ versus Ω_{RF} are presented for three different DC field strengths. Since the maximum value of the applied RF field, $\Omega_{\mathrm{RF}} = 12$ Hz $< 0.5\Omega_0/2\pi$, the analysis was limited to the lowest order of the perturbative expression [3, 4]. According to equation (1), the shift should be inversely proportional to the intensity of the static magnetic field and increase quadratically with the amplitude of the modulated magnetic field, These predictions are well confirmed with the data presented in figure 4. However, an anomaly of unknown origin is seen around $\Omega_{\mathrm{RF}}/(2\pi) = 2.5$ Hz, where experimental BSS value seem to be amplified.

In figure 5, the resonance position is shown for both rotating and oscillating AC field as the function of Ω_{RF} ($\Omega_0/(2\pi) = 45$ Hz). Solid red (or grey) and dashed black lines represent numerical solutions while dots and squares are experimental datapoints. Experimental dependencies agree well with the theoretical curves. Particularly, the resonance position barely depends on the AC-field Rabi frequency for rotating-field-induced

[7] Typically uncompensated field is of order of 10 μG (10^{-9} T).

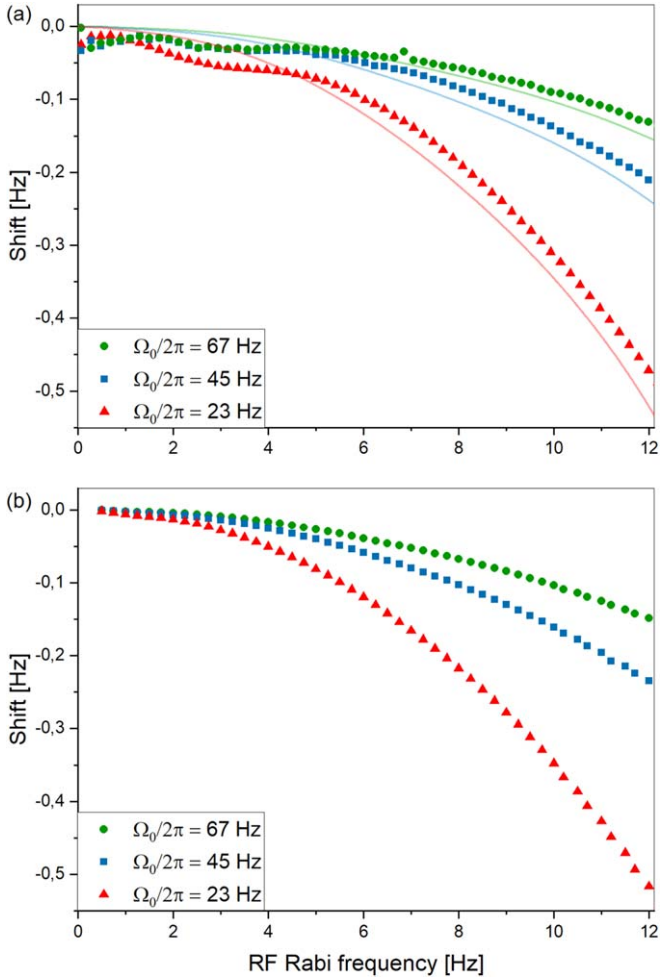

Figure 4. Results of (a) experiment and (b) numerical calculations performed for three different Larmor frequencies. Polynomial fits from numerical data are shown in experimental section (a) as solid lines. The shift depends quadratically (first-order approximation) on the RF Rabi frequency and scales inversely with the static magnetic-field strength. The negative value of the shift reflects conversion from the static magnetic field sweeping to the frequency sweeping of the AC field.

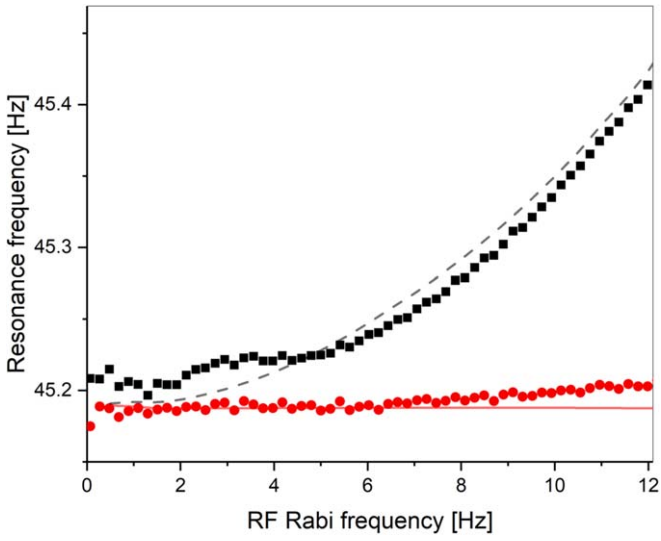

Figure 5. Resonance position as the function of Ω_{RF} for oscillating (black squares) and rotating magnetic fields (red or grey dots) at a static magnetic field of $\Omega_0/(2\pi) = 45$ Hz. Solid and dashed lines represent numerical solutions while squares and dots are experimental datapoints.

resonances, which illustrates efficient elimination of BSS. Experimentally measured BSS values appear slightly overestimated by the numerical results. A small systematic shift of the rotating-field results is most likely caused by the magnetic-coil asymmetry (non-zero oscillating component along the DC field) and correspondingly weaker RF modulation of the atomic polarization. Additionally, imbalance of two counter-rotating magnetic-field components in the rotating-field measurements, i.e. some degree of ellipticity, may lead to non-zero signal at $-\Omega_r$ and hence algebraic shift of the resonance.

5. Conclusions

In conclusion, we have characterized the Bloch-Siegert shift (BSS) of magneto-optical resonances in a multilevel ($F \geqslant 1$) system of Rb atoms ($F = 3 \rightarrow F'$ transition in ^{85}Rb) in a parameter range characteristic for precision measurements of nonlinear magneto-optical rotation. The most prominent effect is the evidence of a double resonance structure with features at $-\Omega_r$ and $+\Omega_r$ for the oscillating field and only one resonance $+\Omega_r$ for the rotating field. Various features of the observed signals, such as the BSS, Majorana reversal, phase mixing, and additional resonances due to field inhomogeneity have been investigated both experimentally and theoretically. Taking into account systematic errors discussed in previous sections, as well as simplicity of our theoretical model, a reasonably good agreement with our numerical simulations based on the density-matrix calculations, was obtained.

This study improves our understanding of the processes of light interaction with energy-level structures with with $F > 1/2$. In addition to accurate characterization of the observed resonances, including their distortions, and demonstration of RWA limitations, a method not explored before in context of magneto-optical resonances in room-temperature alkali metal vapors was proposed to mitigate the BSS. Namely, the application of the rotating, rather than oscillating RF field with attenuated amplitude.

While our analysis is focused on magnetometric applications, this work presents a general novel platform to investigate energy-level structures richer than a simple two-level system (qubit) and may apply to many precision measurements beyond RWA with resonance techniques and multilevel systems. Specifically, the precision experiments aiming at searches for permanent electric dipole moment [39] and time-variation of fundamental constants [40] can benefit from the above analysis. Proper accounting for the discussed shifts and/or distortions of the resoance shapes will improve accuracy of NMR [41], quantum magnetometry and metrology. In field of coherent control and quantum information, the above analysis should faciliate state manipulation and information processing with strong fields and high transmission rates in atoms, solids, as well as, in circuit QED and new materials.

Acknowledgments

This article is dedicated to the memory of Professor Jerzy Zachorowski. The authors would like to acknowledge stimulating discussion with Dmitry Budker and Derek F Jackson Kimball. SP and WG would like to recognize funding from the Polish National Centre of Science (grants 2015/19/B/ST2/02129, 2012/07/B/ST2/00251, 2016/21/B/ST7/01430).

ORCID iDs

J I Sudyka https://orcid.org/0000-0001-5690-1471
S Pustelny https://orcid.org/0000-0003-3764-1234
W Gawlik https://orcid.org/0000-0002-9886-5736

References

[1] Bloch F and Siegert A 1940 Magnetic resonance for nonrotating fields *Phys. Rev.* **57** 522
[2] Cohen-Tannoudji C, Dupont-Roc J and Fabre C 1973 A quantum calculation of the higher order terms in the Bloch–Siegert shift *J. Phys. B: At. Mol. Phys.* **6** L214
[3] Shirley J H 1965 Solution of the schroedinger equation with a Hamiltonian periodic in time *Phys. Rev.* **138** 979
[4] Hannaford P, Pegg D T and Series G W 1973 Analytical expressions for the Bloch–Siegert shift *J. Phys. B: At. Mol. Phys.* **6** L222
[5] Arimondo E and Moruzzi G 1973 Bloch–Siegert shift in optically oriented Hg(199) vapour *J. Phys. B: At. Mol. Phys.* **6** 2382
[6] Arimondo E and Moruzzi G 1982 Aligned atoms in a strong oscillating RF field. A simple treatment by continued fraction of 2 × 2 matrices *J. Phys. B: At. Mol. Phys.* **15** 73
[7] Mehring M, Hoefer P and Grupp A 1986 Bloch–Siegert shift, Rabi oscillation, and spinor behavior in pulsed electron-nuclear double-resonance experiments *Phys. Rev.* A **33** 3523
[8] Emsley L and Bodenhausen G 1990 Phase shifts induced by transient Bloch–Siegert effects in NMR *Chem. Phys. Lett.* **168** 297
[9] Sacolick L, Wiesinger F, Hancu I and Vogel M W 2010 B_1 mapping by Bloch–Siegert shift *Magn. Reson. Med.* **63** 1315
[10] Forn-Diaz P, Lisenfeld J, Marcos D, Garcia-Ripoll J J, Solano E, Harmans C J and Mooij J E 2010 Observation of the Bloch–Siegert shift in a qubit-oscillator system in the ultrastrong coupling regime *Phys. Rev. Lett.* **105** 237001

[11] Pietikäinen I, Danilin S, Kumar K S, Vepsäläinen A, Golubev D S, Tuorila J and Paraoanu G S 2017 Observation of the Bloch–Siegert shift in a driven quantum-to-classical transition *Phys. Rev.* B **96** 020501(R)
[12] Fuchs G D, Dobrovitski V V, Toyli D M, Heremans F J and Awschalom D D 2009 Gigahertz dynamics of a strongly driven single quantum spin *Science* **326** 1520
[13] Scheuer J *et al* 2014 Precise qubit control beyond the rotating wave approximation *New J. Phys.* **16** 093022
[14] Laucht A *et al* 2016 Breaking the rotating wave approximation for a strongly driven dressed single-electron spin *Phys. Rev.* B **94** 161302(R)
[15] Hofferberth S, Fischer B, Schumm T, Schmiedmayer J and Lesanovsky I 2007 Ultracold atoms in radio-frequency dressed potentials beyond the rotating-wave approximation *Phys. Rev.* A **76** 013401
[16] Garraway B M and Perrin H 2016 Recent developments in trapping and manipulation of atoms with adiabatic potentials *J. Phys. B: At. Mol. Opt. Phys.* **49** 172001
[17] Bentine E, Harte T L, Luksch K, Barker A J, Mur-Petit J, Yuen B and Foot C J 2017 Species-selective confinement of atoms dressed with multiple radiofrequencies *J. Phys. B: At. Mol. Opt. Phys.* **50** 094002
[18] Sie E J *et al* 2017 Large, valley-exclusive Bloch–Siegert shift in monolayer WS_2 *Science* **355** 1066
[19] Budker D, Gawlik W, Kimball D F, Rochester S M, Yashchuk V V and Weis A 2002 Resonant nonlinear magneto-optical effects in atoms *Rev. Mod. Opt.* **74** 1153
[20] Budker D and Jackson Kimball D F 2013 *Optical Magnetometry* (Cambridge: Cambridge University Press)
[21] Grujić Z D, Koss P A, Bison G and Weis A 2015 A sensitive and accurate atomic magnetometer based on free spin precession *Eur. Phys. J.* **69** 135
[22] Jammi S, Pyragius T, Bason M G, Florez H M and Fernholz T 2018 Dispersive detection of radio-frequency-dressed states *Phys. Rev.* A **97** 043416
[23] Sycz K, Wojciechowski A M and Gawlik W 2018 Atomic-state diagnostics and optimization in cold-atom experiments *Sci. Rep.* **8** 2805
[24] Ledbetter M, Acosta V M, Rochester S M and Budker D 2007 Detection of radio frequency magnetic fields using nonlinear magneto-optical rotation *Phys. Rev.* A **75** 023405
[25] Zigdon T, Wilson-Gordon A D, Guttikonda S, Bahr E J, Neitzke O, Rochester S M and Budker D 2010 Nonlinear magneto-optical rotation in the presence of radio-frequency field *Opt. Express* **18** 25494
[26] Gawlik W and Pustelny S 2009 Nonlinear Faraday effect and its applications *New Trends in Quantum Coherence and Nonlinear Optics* ed R Drampyan vol 263 (New York: NOVA Science Publishers) pp 45–82
[27] Molina-Terriza G, Vaziri A, Rehacek J, Hradil Z and Zeilinger A 2004 Triggered qutrits for quantum communication protocols *Phys. Rev. Lett.* **92** 167903
[28] Auzinsh M, Budker D and Rochester S 2010 *Optically Polarized Atoms* (Oxford : Oxford University Press)
[29] Rochester S *Mathematica* ADM package http://rochesterscientific.com/ADM/
[30] Yashchuk V V, Lee S K and Paperno E 2013 Magnetic shielding *Optical Magnetometry* ed D Budker and D F Jackson Kimball (Cambridge: Cambridge University Press) ch 12
[31] Corwin K L, Lu Z, Hand C F, Epstein R J and Wieman C E 1998 Frequency-stabilized diode laser with the Zeeman shift in atomic vapor *Appl. Opt.* **37** 3295
[32] Kostinski N, Olsen B A, Marsland R III, McGuyer B H and Happer W 2011 Temperature-insensitive laser frequency locking near absorption lines *Rev. Sci. Instrum.* **82** 33114
[33] Zhivun E, Wickenbrock A, Sudyka J, Pustelny S, Patton B and Budker D 2016 Vector light shift averaging in paraffin coated alkali vapor cells *Opt. Express* **24** 15383
[34] Brossel J and Bitter F 1952 A new double resonance method for investigating atomic energy levels. Application to Hg $^3P_1^*$ *Phys. Rev.* **86** 308
[35] Majorana E 1932 Atomi orientati in campo magnetico variabile *Nuovo Cimento* **9** 43
[36] Pegg D J and Series G W 1973 On the reduction of a problem in magnetic resonance *Proc. R. Soc.* A **332** 281
[37] Cohen-Tannoudji C and Guery-Odelin D 2011 Advances in atomic physics: an overview *Optical Methods* (Singapore: World Scientific) ch 3
[38] Weis A, Bison G and Pazgalev A S 2006 Theory of double resonance magnetometers based on atomic alignment *Phys. Rev.* A **74** 033401
[39] Altarev I *et al* 2010 An improved measurement of the electric dipole moment of the neutron *Nucl. Phys.* A **844** 47C
[40] Leefer N, Weber C T M, Cingöz A, Torgerson J R and Budker D 2013 New limits on variation of the fine-structure constant using atomic dysprosium *Phys. Rev. Lett.* **111** 060801
[41] Trahms L and Burghoff M 2010 NMR at very low fields *Magn. Reson. Imaging* **28** 1244